Bio-cleaned Lignin-based Carbon Fiber and Its Application in Adsorptive Water Treatment

Jiawei Chen[1], Tanushree Ghosh[1,2], Cagri Ayranci[1*], and Tian Tang[1*]

[1]Department of Mechanical Engineering, University of Alberta, 116 St & 85 Ave, Edmonton, Alberta, Canada

[2]Center for Earth Sciences, Indian Institute of Science, C V Raman Rd, Bangalore, Karnataka 560012, India

[*]Corresponding Author: tian.tang@ualberta.ca; cayranci@ualberta.ca; Tel: +1 780 492 5467 Tel: +1 780 492 2791

Abstract

Although an agricultural byproduct, lignin can be a felicitous choice serving as a carbon fiber precursor upon bio-cleaning with *Pseudomonas fluorescence*. In this study, carbon fiber produced from electrospun bio-cleaned lignin (Bio-KLB) was demonstrated to be a novel efficient adsorbent for methylene blue in wastewater treatment. Bio-cleaning effectively changed lignin from un-electrospinnable to easily-electrospinnable by removing impurities. Bio-KLB carbon fiber mats showed average fiber diameter of 278.95±49.89 nm, and randomly dispersed fiber mats showed average elastic modulus of 1532.87±439.63 MPa and tensile strength of 16.72±5.21 MPa. Adsorption of methylene blue on Bio-KLB carbon fibers was analyzed at pH = 9, where optimal adsorption and decent reusability were observed. Kinetic adsorption was fitted well with pseudo-first-order model while adsorption isotherms were fitted to both Langmuir and Freundlich models. The highest adsorption capacity was 548.65 mg/g based on Langmuir model. The results provide clear evidence that electrospun bio-cleaned lignin-based carbon fibers can be a strong alternative material for dye treatment.

1. Introduction

Dyes are colorants binding to surfaces to alter product appearances for textile [1], photo printing [2], plastics [3], food and drug industries [4]. Releasing industrial dyes into water weakens photosynthesis or light penetration of water, depletes oxygen from water, and provokes adverse effects on human health [5]. Some dyes can cause skin irritation, organ dysfunction, allergic dermatitis, or mutation [6]. Methylene blue (MB), an extensively used cationic dye, can induce anemia, hypertension, and nausea [7]. Thus, removal of dyes from wastewater is imperative for ensuring environmental safety. Common dye removal techniques include solvent extraction [8,9], electrolysis [5], electrochemical reactions [10], photocatalytic decolorization [11], ultrafiltration [12], and adsorption [13]. Most of these methods are expensive, demand specialized equipment, generate toxic byproducts, or are unable to manage complete extraction of dyes. However, dye removal by adsorption is of particular research interest because it is cost-effective, easy to operate, and efficient [14]. The conventional adsorbent is commercial activated carbon adopted by most textile industries [15]; however, it may include relatively high-cost material. The present study evaluated a promising low-cost sustainable alternative to commercial activated carbon.

Carbons from sustainable precursors, such as agricultural byproducts or locally available natural resources have attracted considerable research interests as adsorbents for water treatment [16–19]. Lignin, the most abundant aromatic biomass, is one such bio-sustainable resource and a potential alternative precursor for carbon fiber (CF). Lignin is extracted from black liquor, a byproduct from pulp and paper industry. Among various types of lignin, kraft lignin (KL) is widely researched due to its high purity and yield [20]. In the pulp mills, lignin is recycled as fuel [21]; on the other hand, its low cost, sustainability and copious availability make lignin a promising candidate for producing value-added materials such as CF.

Electrospinning is a commonly employed and highly tailorable production method for fabricating submicron fibers. Electrospun fibers have been extensively studied for the adsorption of dyes, especially MB. Zhao et al. reported that electrospun β-Cyclodextrin-based nanofibers exhibited maximum adsorption capacity of 826.45 mg/g for MB and good recyclability [22]. The adsorption capacity of the nanofibers was exceptional with reported tensile strength of 2.28±0.12 MPa. Submicron to nanoscale lignin-based CF mats produced from electrospinning are porous with large surface area, which are desirable characteristics for adsorbents as they allow for high loading of catalyst-adsorbate system and large mass flux [23]. Beck et al. proposed to use carbon

nanofibers electrospun from commercial lignin and polyvinyl alcohol (PVA) as dye adsorbent [24]. PVA was used as a spinning aid to accommodate low-molecular-weight lignin. The maximum adsorption capacity was 220 mg/g for MB which, although lower than the value reported by [22], was much higher than electrospun PAN-based carbon nanofibers, activated carbon, and carbon nanotube [25]. While the mechanical properties of the CFs were not reported, the authors demonstrated the feasibility of using this renewable material as potential MB adsorbent for water treatment.

One of the most challenging issues to make lignin-based CF suitable for water treatment is the spinnability of lignin. Lignin is unspinnable by itself due to its low molecular weight (MW), and thus an aiding polymer with higher MW is typically mixed with lignin to improve the spinnability. Impurities such as sodium and carbohydrates also negatively affect the spinnability, leading to defects in the fibers, electrospraying, or complete inability to spin. Common purification methods, such as acid washing or fractionation, generally adopt harsh chemicals that are environmentally unfriendly. To address this problem, a novel process was introduced in our previous work to biodegrade impurities using bacteria *Pseudomonas fluorescence* without modifying the structural integrity of lignin [26,27]. The purification was shown to improve the mechanical properties of the lignin-based CFs produced from kraft lignin A (KLA) [26,27].

In this work, we explore CFs electrospun from bio-cleaned lignin as a low-cost, non-toxic, and biodegradable adsorbent material. We produced electrospun CFs from untreated KLA and bio-cleaned kraft lignin B, while KLB before bio-cleaning was completely unspinnable. The morphologies, mechanical properties, and MB adsorption capacity of the lignin-based CFs were characterized for water treatment application. Figure 1 shows a schematic of process to fabricate lignin-based carbon fibers and use them for MB adsorption.
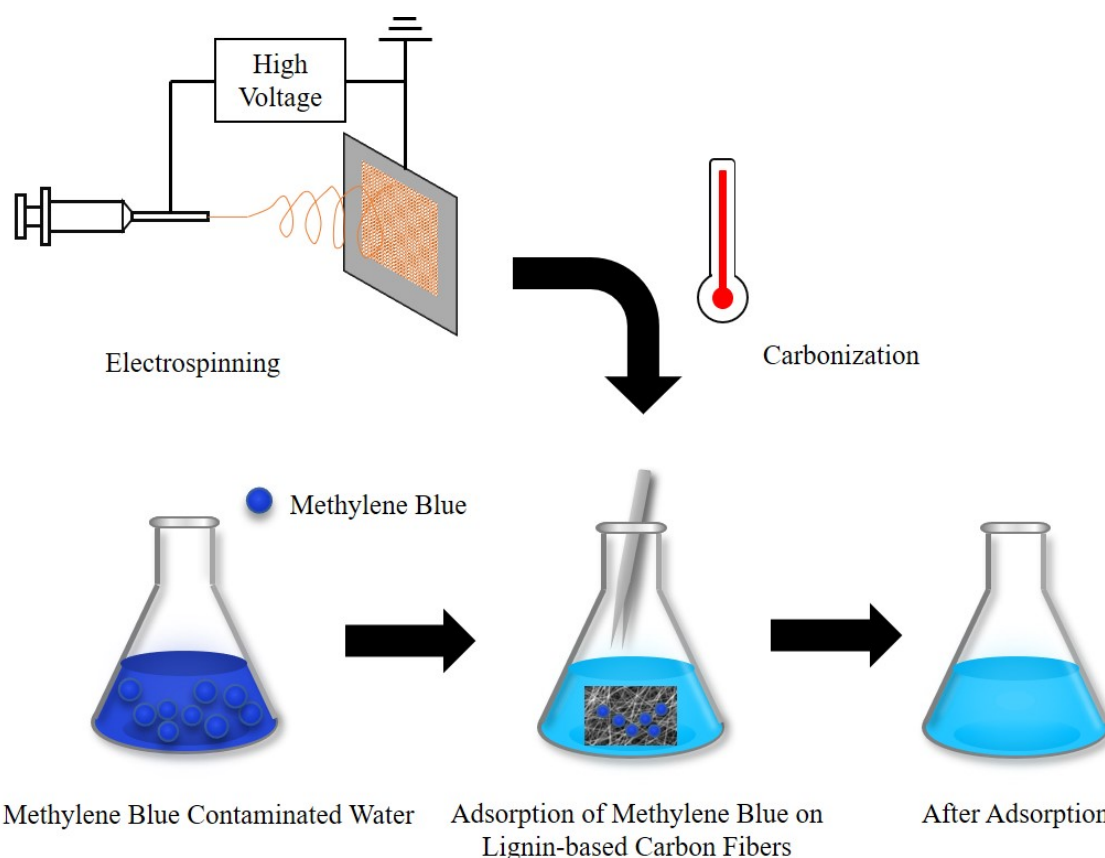
Figure 1. Experimental schematic of fabrication of lignin-based carbon fibers and MB adsorption

2. Materials and Methods

2.1. Materials

KLB and KLA (Amallin^{TM}) were both produced by West Fraser Timber Co. Ltd. and supplied by InnoTech, Alberta. KLA is water-insoluble and acidic, while KLB is water-soluble and alkaline. The bio-cleaning process and optimization of electrospinning were outlined in earlier works [26,27]. Anhydrous grade *N,N*-Dimethylformamide (DMF), Hydrochloric acid (HCl), polyethylene oxide (PEO) with molecular weight of 1000 kDa and MB with molecular weight of 319.85 Da were obtained from Sigma Aldrich, Canada. MB was selected as a model dye to examine the adsorption capacity of CFs. Methanol was purchased from Fisher Scientific.

2.2. Solution Preparation

Lignin samples were dried in a vacuum chamber at 100 °C prior to solution preparation. A small amount of PEO was used as a binding polymer to assist lignin in the electrospinning process. It was first dissolved in DMF at 80 °C and under the stirring rate of 600 rpm to obtain a

uniform solution. Vacuum-dried lignin powder was then added to the PEO solution to achieve an overall solid concentration of 22 wt% and lignin/PEO weight ratio of 95/5 [27]. The same stirring conditions were applied to the solution overnight (12 hours). The solution was cooled to room temperature (RT; 20±2°C) prior to electrospinning.

2.3. Electrospinning

The solution was loaded in a 10 mL syringe (BD PrecisionGlide, Fisher Scientific, Canada). A syringe pump (Geneq Inc., Canada) was used to obtain a feed rate of 420 nl/s [27]. A positive voltage of 14 kV was applied to a blunt needle (20 Gauge) attached to the syringe by a high voltage supplier (GAMMA High Voltage Research, Ormond Beach, FL, USA). The static collector was a grounded plate covered with aluminum foil, located at 20 cm from the needle tip. After collecting for 30 min, the electrospun fiber mat was placed in a fume hood overnight to ensure the residual DMF was fully evaporated. Three fiber mats were produced under each electrospinning condition for further characterization. All lignin samples used for electrospinning are listed in Table 1.

2.4. Thermostabilization and Carbonization

The electrospun lignin fiber mats were cut into 40 mm x 70 mm rectangular strips and placed on a quartz plate. Both thermostabilization and carbonization were performed in a tube furnace (OTF-1500X-UL, Lindberg/Blue M^{TM}, MTI Corporation, USA). The sample was heated at a rate of 0.5 °C/min in air from RT to 250 °C and held at 250 °C for 1 hour [27,28]. It was then brought back to RT while argon was purged through the chamber for 3 hours until air was fully removed. The sample was heated again under argon at the same rate till 250 °C, followed by carbonization where the infusible fibers were heated at a rate of 5 °C/min to 1000 °C and held at 1000 °C for 1 hour. Finally, the sample was cooled to RT and weighed to determine the yield of carbonization.

2.5. Scanning Electron Microscopy and Fiber Analysis

Scanning Electron Microscopy (SEM) samples were acquired from two different regions on each fiber mat to perform fiber morphology characterization. The samples were placed on SEM specimen stubs anchored with carbon tapes and coated with gold (Gold Sputtering Unit DESK II, Denton Vacuum, Moorestown, USA) for 120 sec to prevent charging. Images were taken from various locations on the sample with Zeiss EVO MA10 Microscope (Oberkochen, Germany) under acceleration voltage of 20kV. For each electrospun condition, at least 100 fibers

were measured from SEM images with ImageJ (NIST, ver 1.52 p) to obtain the average fiber diameter. Porosity analysis was conducted using DiameterJ, a plugin of ImageJ [29]. Binary (black and white) images were produced by manually adjusting the thresholds to remove the background. Mean area of the pores was determined by considering at least 3 SEM images of each carbon mat. The equivalent pore diameter was calculated from the pore area using the following equation [30],

$$\text{Equivalent Diameter} = \left(\frac{4 \times \text{Pore Area}}{\pi} \right)^{\frac{1}{2}} \tag{1}$$

2.6. Mechanical Test

Ten 10 mm x 50 mm specimens were cut from each randomly distributed fiber mat, with the longer dimension along the loading direction. Tensile tests were conducted on the specimens using an ElectroForce 3200 Series III tensile tester (Bose Corporation) with a 250 g maximum load cell. Gauge length was 30 mm and strain rate was 0.01 mm/s. Thickness of each sample was calculated following the same procedure as described in our previous work [27]. Strain at failure was determined when the load dropped below 0.1 N.

2.7. Chemical Characterization

Raman Spectra of CF samples were collected using inVia Raman Microscope (Renishaw, UK) with laser wavelength of 532 nm scanned from 800 cm^{-1} to 1800 cm^{-1}. Fourier-transform infrared spectroscopy (FTIR) was used to characterize surface functional groups of the CF samples. FTIR was conducted using NicoletTM iS50 FTIR spectrometer (Thermo Fisher Scientific) with a built-in attenuated total reflectance (ATR) module. Every measurement was obtained with a resolution of 4 cm^{-1} and 32 scans over the range of 400-4000 cm^{-1}. Elemental compositions of the CF samples were determined with X-ray photoelectron spectroscopy (XPS). XPS was conducted using Kratos AXIS Ultra spectrometer with monochromatic Al Kα X-ray source at 1486.7 eV, pass energy of 160 eV for survey scans and pass energy of 20 eV for high resolution scans of C 1s. The XPS spectra were analyzed and deconvoluted with CasaXPS. The binding energies were calibrated with reference to C 1s peak at 284.8 eV.

2.8. Methylene Blue Adsorption Experiments

MB solution was agitated in a shaker (VWR® incubating orbital shaker, VWR International, Canada) operated at 120 rpm. The concentration of MB was determined with Novaspec II spectrophotometer (Pharmacia Biotech, Cambridge, England) at the wavelength of

665 nm. A KLA-C or Bio-KLB-C (see Table 1 for the sample names) mat with mass of 2 mg was submerged into the MB solution for adsorption experiments, with different durations specified later. After extracting the CF mat, 2mL of the MB solution was transferred into a microcentrifuge tube and centrifuged (mini-centrifuge from Fisherbrand™, Fisher Scientific, USA) for 10 mins to remove any suspended CF sample. The supernatant was transported into a cuvette and its light absorbance was measured by spectrophotometer. Absorbance measurement of each solution concentration was repeated three times to obtain the average data. The adsorption experiments were conducted at RT of 20-24°C.

2.8.1. Standard Curve of Methylene Blue

MB is a representative adsorbate that shows resemblance to other polar organic dyes, such as crystal violet and cationic light yellow 7GL [31]; thus it was selected in this study to investigate the adsorption ability of lignin-based CFs. The standard curve of MB was plotted based on the absorbance of MB solutions with known concentration. MB powder was dissolved in deionized (DI) water to produce 30 mL MB solutions with concentrations of 0-200 mg/L in 125 mL glass flasks. The prepared solution was shaken until MB was fully dissolved. The average absorbance was plotted against the corresponding MB concentration and fitted linearly to generate the standard curve.

2.8.2. Effect of pH

Effect of pH on MB adsorption was evaluated by adding 0.1 mol/L HCl or NaOH dropwise to modify the pH (ranging between 3 and 11) of 100 mL MB solution with initial concentration of 40 mg/L. KLA-C and Bio-KLB-C mats were added into each MB solution and agitated until equilibrium was reached. The equilibrium adsorption capacity q_e (mg/g) was calculated from the following equation [32],

$$q_e = \frac{(C_0 - C_e) \times V}{W}$$

(2)

where C_0 (mg/L) and C_e (mg/L) are respectively the initial concentration and the final equilibrium concentration of the MB solution. V (mL) is the volume of MB solution and W (g) is the mass of the adsorbent. Average adsorption capacity was evaluated at different pH levels to find the optimal pH for adsorption.

2.8.3. Kinetic Adsorption Experiments

Using the optimal pH determined from Section 2.7.2, CF mat was immersed in 100 mL MB solution (initial concentration of 40 mg/L). The MB solution was agitated and 2 mL was extracted at different time to measure the adsorption capacity

$$q_t = \frac{(C_0 - C_t) \times V}{W} \qquad (3)$$

where C_t is the concentration of the MB solution at the time of extraction t (min). The extraction was performed once every 5 mins for the first 30 mins (0, 5, 10, 15, 20, 25, 30 mins) and once every hour afterwards (1, 2, 3, 4, 5 hours). The measured adsorption capacities were plotted against time and fitted with the pseudo-first-order model and pseudo-second-order model [33]. Pseudo-first-order model is given by,

$$q_t = q_e - q_e \times \exp(-K_1 t) \qquad (4)$$

where K_1 is the rate constant for the pseudo-first-order equation. Pseudo-first-order model assumes that the dominating adsorption mechanism is physical (physisorption). Pseudo-second-order model is given by,

$$q_t = \frac{K_2 q_e^2 t}{1 + K_2 q_e t} \qquad (5)$$

where K_2 is the rate constant for the pseudo-second-order equation. Pseudo-second-order model assumes that the dominating adsorption mechanism is chemical (chemisorption). The time to reach equilibrium adsorption capacity was determined from kinetic adsorption experiments.

2.8.4. Batch Adsorption Experiments

After finding the time to reach equilibrium adsorption, CF mats were submerged into 100 mL MB solutions with initial concentrations of 1-40 mg/L at the optimal pH level. The solution was agitated until equilibrium. The equilibrium adsorption capacity averaged from 3 tests was plotted against different solution concentrations to determine the adsorption isotherm, which was then fitted with the Langmuir model and Freundlich model [34]. Langmuir adsorption isotherm assumed that maximum adsorption took place as the adsorbate formed a saturated monolayer on a homogeneous adsorbent surface with constant adsorption energy and no transmigration of adsorbate occurred [35,36]. Freundlich adsorption isotherm assumed that adsorption occurred on a heterogeneous absorbent surface with exponential distribution of adsorption energies [36]. Langmuir model is given by,

$$q_e = \frac{q_{max} K_L C_e}{1 + K_L C_e} \tag{6}$$

where q_{max} is the maximum adsorption capacity and K_L is the equilibrium constant. Freundlich model is given by,

$$q_e = K_F C_e^{\frac{1}{n}} \tag{7}$$

where K_F and n are Freundlich constants that indicate adsorption capacity and adsorption intensity, respectively.

2.8.5. Cyclic Adsorption Experiments

The reusability of CF mat was assessed by immersing the CF mat adsorbed with dye (40 mg/L) from batch adsorption experiments into methanol solution with 5% 0.1 M HCl (v/v) for 3 hours [32]. After desorption, CF mat was washed with DI water and dried in air overnight. Then dried CF mat was submerged into 40 mg/L MB solution again for adsorption. This process was repeated 5 times to evaluate the cyclic adsorption efficiency of the CF mat, which is an assessment of its reusability.

3. Results and Discussion

3.1. Spinnability

Before bio-cleaning, KLB formed a gel-like solution at 22 wt% of solid. The impurities within KLB increased the viscosity of the solution and prohibited it from electrospinning. Reducing the total solid concentration was insufficient to enable the spinnability of KLB. After bio-cleaning with *Pseudomonas fluorescence*, ash and carbohydrate content were reduced by 99% and 57% respectively without affecting lignin [26]. These impurities negatively influenced solubility of lignin in the solvent, adversely affected electrospinning, and posed undesirable impact on carbon yield and mechanical properties of the produced lignin-based CFs [37,38]. Bio-KLB solution was able to be electrospun into uniform fibers at 70 kV/m. The transition of spinnability demonstrated the effectiveness of bio-cleaning in purifying lignin for electrospinning purpose.

3.2. Fiber Morphology

SEM images of electrospun and carbonized Bio-KLB fibers before and after MB adsorption are shown in Figure 2. Corresponding images for KLA have been reported in [27]. Bio-

KLB electrospun fibers were uniform and cylindrical (Figure 2a); only a few porous beads and irregular lumps were observed (Figure 2b) similar to the findings reported by Aslanzadeh et al. [39,40]. Average diameter of Bio-KLB fibers reduced from 421.58±59.47 nm after electrospinning to 278.95±49.89 nm after carbonization. The fiber diameter of Bio-KLB-C was 58% smaller than that of KLA-C [27]. The small fiber diameter of Bio-KLB-C was crucial in dye adsorption since it reduced the probability of solvent entrapment that could induce bead formation [41]. After adsorption, the fiber morphology did not change but average fiber diameter increased up to 1.24 times of the original size (Figure 2d), indicating that MB particles were adsorbed onto the surface of Bio-KLB-C.

Table 1

Information on the electric field used and diameter of the as-spun and carbonized fibers

Name	Sample	Electric Field (kV/m)	Fiber Diameter (nm)	Ref
KLA	Electrospun untreated KLA	50	1000.48 ± 97.48	[27]
KLA-C	Carbonized untreated KLA	50	663.17 ± 64.51	[27]
Bio-KLB	Electrospun bio-cleaned KLB	70	421.58±59.47	This work
Bio-KLB-C	Carbonized bio-cleaned KLB	70	278.95±49.89	This work
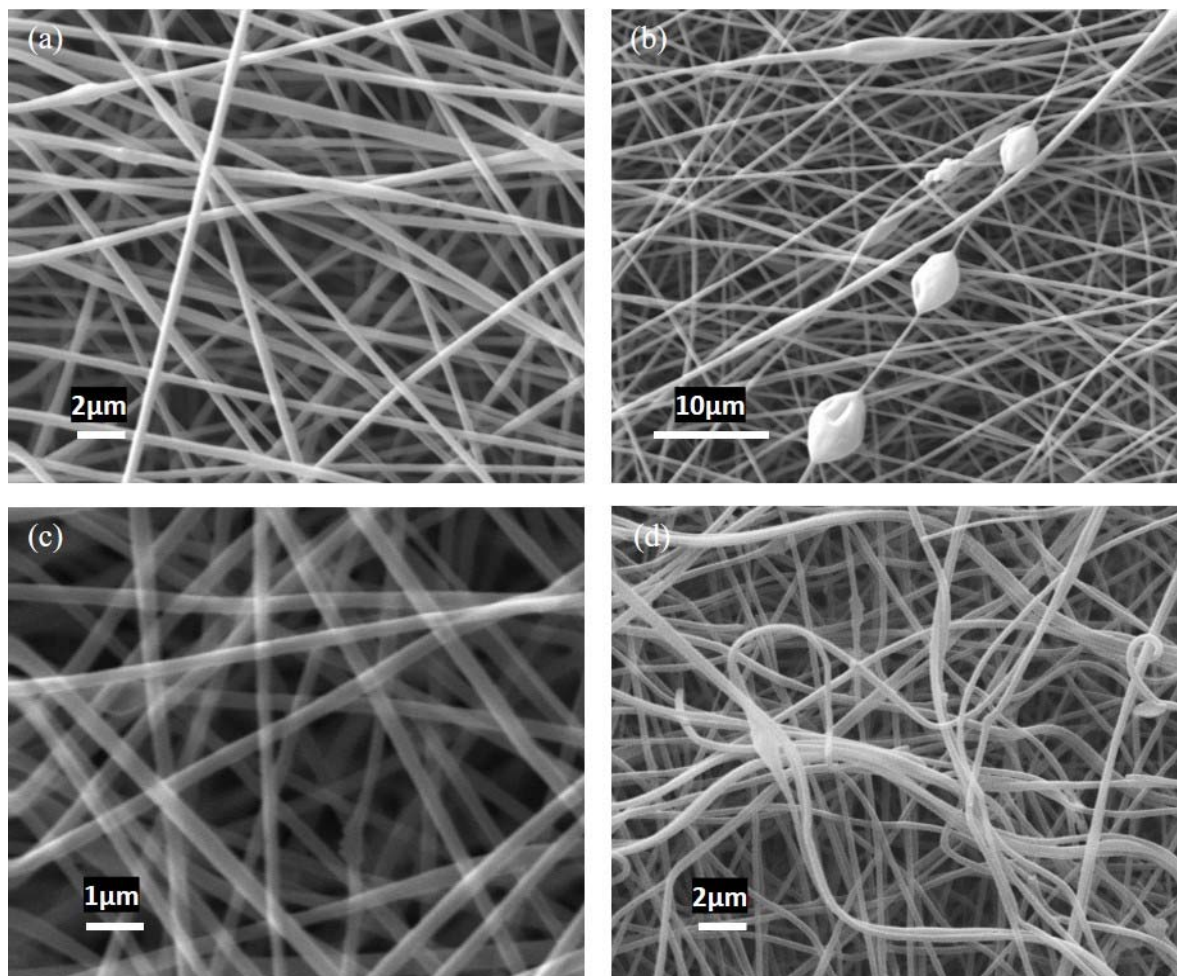
Figure 2. Fiber morphology of (a) electrospun Bio-KLB with uniform fibers, (b) electrospun Bio-KLB with beads, (c) Bio-KLB-C fibers before adsorption, and (d) Bio-KLB-C fibers after adsorption

Mean mat pore area, porosity obtained from DiameterJ, and calculated equivalent pore diameter are summarized in Table 2. Even though pore size of Bio-KLB-C was smaller compared to KLA-C, smaller fiber diameter and larger porosity for Bio-KLB-C drastically enlarged the surface area for adsorption [42]. The pores were large enough for MB molecules to diffuse into the mat and the greater surface area provided a larger number of potential reaction sites for MB adsorption.

Table 2

Measured pore properties for KLA-C and Bio-KLB-C mats

Name	Mean Pore Area (nm^2)	Porosity (%)	Equivalent Pore Diameter (nm)
KLA-C	1661.6	37.13	46.00
Bio-KLB-C	271.6	66.55	18.59

3.3. Mechanical Properties

Mechanical properties of the lignin fiber mats are compared in Figure 3. Representative stress-strain curves are presented in Figure S1 (see Supporting Information). All lignin fibers manifested substantial decrement in the strain at failure after carbonization, indicating reduction in fiber ductility caused by carbonization. Tensile strength of Bio-KLB fibers showed 2-fold increase after electrospinning and 3-fold increase after carbonization, compared to KLA fibers. Average elastic modulus of Bio-KLB-C showed 1.7-fold increase from KLA-C. These data indicated bio-cleaning not only improved spinnability of KLB by removing the impurities like ash and carbohydrates [26], but also enhanced mechanical properties of lignin fibers. High mechanical performance is favored for adsorbents in practical water treatment applications, especially in industrial processes where high durability is required in order to prevent tear and other damages [43,44]. The excellent mechanical properties demonstrated here make Bio-KLB-C a durable adsorbent with high structural integrity suitable for a wide range of applications.
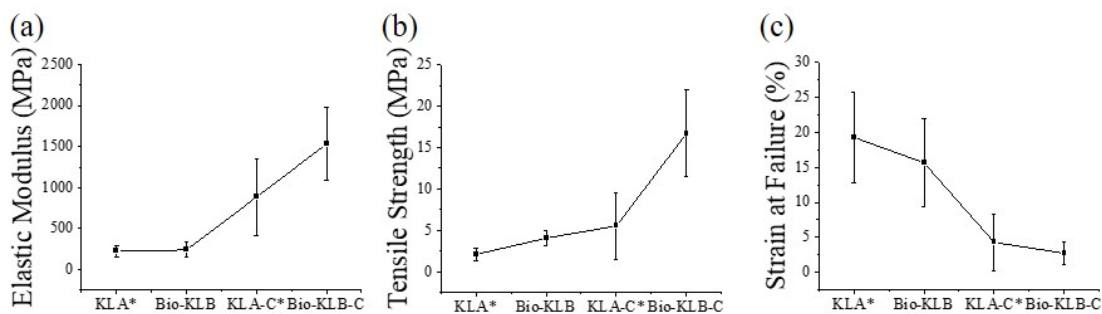
Figure 3. Mechanical properties, including (a) elastic modulus, (b) tensile strength, and (c) strain at failure of lignin fibers after electrospinning and carbonization with data of KLA and KLA-C (*) reported in previous work [27]

3.4. MB Adsorption

3.4.1. pH Effect and Kinetic Adsorption

The effect of pH on the equilibrium adsorption capacity of MB on KLA-C and Bio-KLB-C is shown in Figure 4a. After submerging CF mat into 40 mg/L MB solution, the reactions of KLA-C and Bio-KLB-C to pH showed qualitative similarity but significant quantitative differences. High adsorption capacity of MB on CF has been reported at both low and high pH levels in other literatures for different precursors [45,46]. In this work, equilibrium adsorption capacity for KLA-C increased as pH changed from 3 to 5, reached maximum at pH = 5, and decreased as the solution became more alkaline (pH>5). The overall equilibrium adsorption capacity of MB on KLA-C was much lower compared to that of Bio-KLB-C, and the variation with pH was insignificant.

The equilibrium adsorption capacity of MB on Bio-KLB-C experienced much more drastic changes with pH compared to KLA-C: slight increase with pH from 3 to 5, rapid rise until the peak at pH = 9, and gradual decrease as pH level further increased. The weak adsorption at low pH level could be attributed to protonated MB at triplet state competing with free H^+ ions to the adsorption sites of Bio-KLB-C [45,47]. As pH level elevated, reduction of surface charge promoted adsorption of cationic MB. The transition from increasing to decreasing trends of the adsorption capacity curve corresponded to the optimal pH at which the adsorption performance was the best.

The optimal pH level was applied for subsequent kinetic adsorption experiments. The changes in kinetic adsorption capacity with respect to time are shown in Figure 4b and 4c for KLA-C and Bio-KLB-C, respectively. The data were fitted using non-linear pseudo-first-order model and pseudo-second-order model with constant parameters, and the correlation coefficients (R^2) are summarized in Table 3. For KLA-C, a slight increase in kinetic adsorption capacity was observed in the first 30 mins. However, the standard deviation of the data in Figure 4b was so large that the change in data can be concluded to be statistically insignificant. Neither models fitted the data well, with low R^2, due to the small variation of the adsorption capacity with time.

Table 3

Kinetic Adsorption Model Parameters for KLA-C and Bio-KLB-C

Adsorbent	Pseudo-first-order model			Pseudo-second-order model			Experimental
	q_e (mg/g)	K_1 (1/min)	R^2	q_e (mg/g)	K_2 (1/min)	R^2	q_e (mg/g)
KLA-C	3.80	0.21	0.15	3.93	0.14	0.52	3.94
Bio-KLB-C	174.16	0.02	0.96	214.50	1.02 E-4	0.94	168.97

In terms of Bio-KLB-C, kinetic adsorption capacity increased briskly and saturated after 180 min (3 hours), indicating the attainment of equilibrium. From Figure 4c, the pseudo-first-order and pseudo-second-order models both fit the kinetic adsorption data of Bio-KLB-C well with R^2 of 0.96 and 0.94 respectively. The equilibrium adsorption capacity predicted by the pseudo-first-order model was closer to the experimental value. The good agreement between the data and these two models suggested physisorption (pseudo-first-order model) and chemisorption (pseudo-second-order model) both affected the adsorption of MB on Bio-KLB-C [48]. The fitting was better with the pseudo-first-order model, suggesting physisorption was more dominant. The small Bio-KLB-C fiber diameter assisted in the physisorption of MB as demonstrated in the SEM characterization.

It is clear from Figure 4 that the adsorption capacity of MB on KLA-C was much lower than that of Bio-KLB-C. In consideration of its low adsorption capacity and large standard deviations observed in Figure 4b, adsorption isotherm experiment was not conducted for KLA-C. For Bio-KLB-C, adsorption isotherm tests were conducted for the duration of 3 hours, which was the time required to reach equilibrium in kinetic adsorption (Figure 4c).
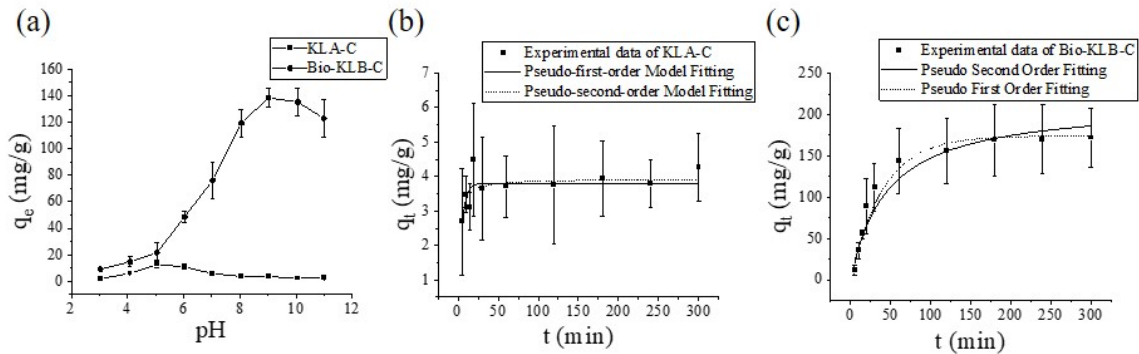
Figure 4. (a) Effect of pH on the equilibrium adsorption capacity of MB on KLA-C and Bio-KLB-C, (b) kinetic adsorption of MB on KLA-C and (c) kinetic adsorption of MB on Bio-KLB-C, both fitted with pseudo-first-order model and pseudo-second-order model

14

3.4.2 Chemical Characterization

Raman and FT-IR spectra of KLA-C and Bio-KLB-C are shown in Figure 5. In the Raman spectra (Figure 5a), the D band and G band were found at 1325-1335 cm^{-1} and 1590-1600 cm^{-1}, respectively. D band corresponded to vibration mode of sp^3 hybridized carbon and G band corresponded to idealized sp^2 hybridized carbon [49]. The intensity ratio (I_D/I_G) between D band and G band was 0.87 for KLA-C and 0.90 for Bio-KLB-C, indicating both samples mainly consisted of amorphous carbon. However, I_D/I_G of both samples was lower than I_D/I_G of CF produced from sulfur free softwood lignin, suggesting lignin-based CFs reported in this study possessed higher degree of graphitization [28].

In the FTIR spectra (Figure 5b), small peaks between 675 and 900 cm^{-1} were attributed to C-H out-of-plane bending [50]. The 1070-1200 cm^{-1} band was attributed to C-O stretching of alcoholic or phenolic groups in CF, or axial deformation of C-N of aliphatic amines in MB [50,51]. After reaching equilibrium adsorption capacity, the peaks at 1120~1150 cm^{-1} slightly shifted for both KLA-C and Bio-KLB-C to 1140 cm^{-1}, indicating the C-N/C-O functional groups participated in the interaction with MB molecules. The peaks at 1570-1580 cm^{-1} could be due to C=C stretching in aromatic rings [52]. The peaks in the range of 1700-1900 cm^{-1} corresponded to carboxylic acid groups and the peaks at 2100 cm^{-1} were attributed to the C=C=C groups [53,54].

The surface functional groups of the CF samples before and after adsorption were characterized with XPS. The XPS spectra (Figure 5c) showed that before the adsorption, KLA-C consisted of 79.66% C and 20.34% O, while Bio-KLB-C consisted of 74.39% C and 25.61% O. After adsorption, N 1s and S 2p appeared for KLA-C and Bio-KLB-C. These elements did not exist before the adsorption, which indicated adsorption of MB on the surface of the CF samples. The increase in nitrogen content was ascribed to cationic MB-N+ group [55]. The oxygen content decreased to 13.92% for KLA-C and 18.06% for Bio-KLB-C. The C 1s spectra (Figure 5d) were deconvoluted to C-C/C-H at 284.8 eV, C-O at 285.4 eV, C-N/C-O at 286.1 eV, and O-C=O at 288.7 eV [56–59]. C-N/C-O increased from 26.39% to 39.80% for KLA and from 23.83% to 42.05% for Bio-KLB-C, demonstrating chemisorption of MB on the surface.

The occurrence of chemisorption explained the good fitting of kinetic adsorption curve for Bio-KLB-C with the pseudo-second-order model in Section 3.4.1. In alkaline solution, the surface functional groups on Bio-KLB-C such as the carboxyl group were deprotonated to promote cationic MB-N+ groups to be attracted to the CF samples. But in acidic solution, these

functional groups were protonated to repulse cationic MB [55]. Therefore, the equilibrium adsorption capacity of MB on Bio-KLB-C maximized in alkaline environment (Figure 4a). On the other hand, the pseudo-first-order model provided even better fitting to the kinetic adsorption curve of Bio-KLB-C, suggesting that physisorption might be a more dominant adsorption mechanism. The much smaller fiber diameter of Bio-KLB-C provided more adsorption sites for MB, which caused the MB adsorption capacity of Bio-KLB-C to surpass that of KLA-C.
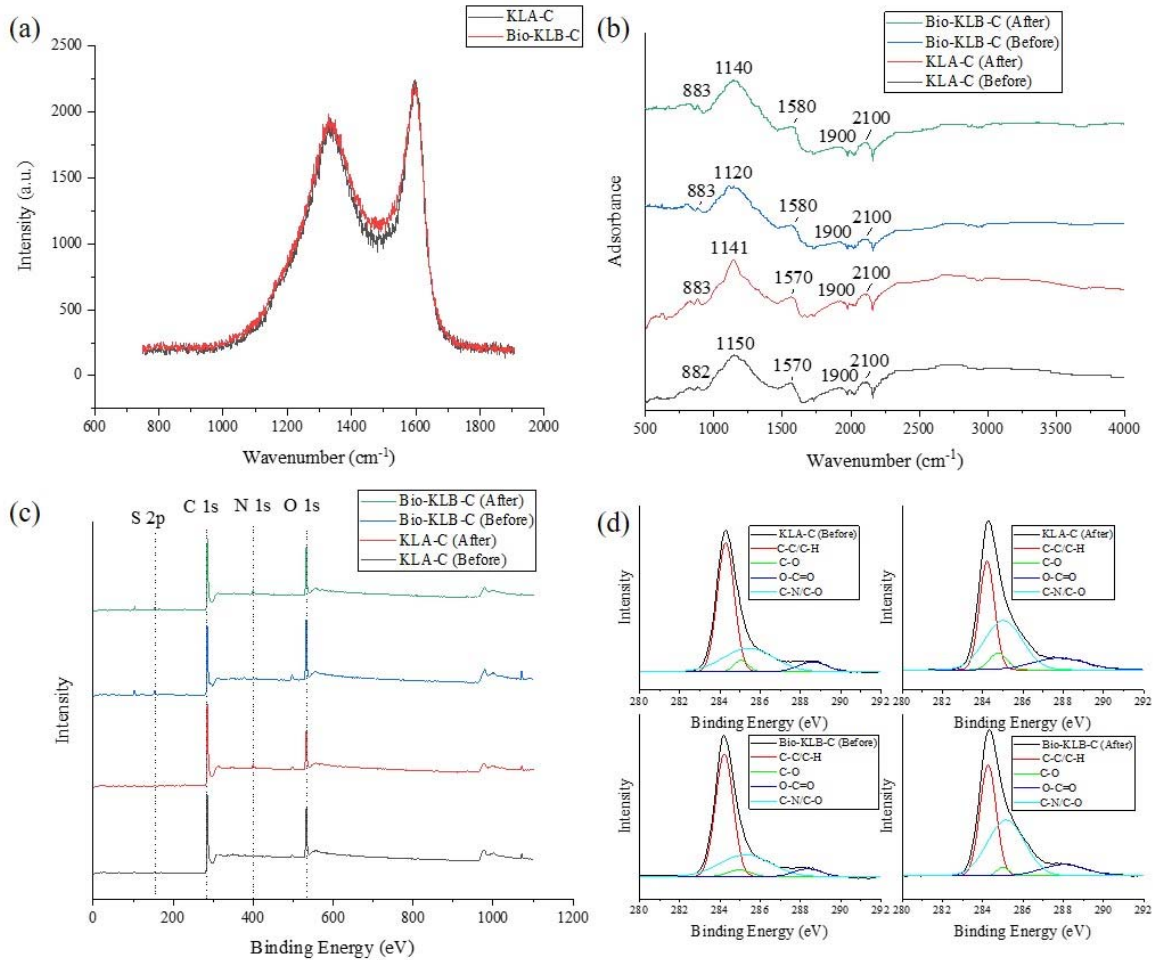
Figure 5. (a) Raman spectra of KLA-C and Bio-KLB-C before MB adsorption, as well as (b) FTIR (c) XPS survey spectra (d) C1s of the CF samples before MB adsorption and after reaching the equilibrium adsorption capacity

3.4.3. Adsorption Isotherm

To analyze adsorption isotherm, Bio-KLB-C mats were used to adsorb MB in solutions with initial concentration of 1-40 mg/L at the optimal pH of 9 for 3 hr. Langmuir and Freundlich adsorption isotherm models were used to fit the data with parameters listed in Table 4. The adsorption isotherm of Bio-KLB-C with fitted models is shown in Figure 6a. The plot illustrates the relationship between equilibrium adsorption capacity and equilibrium MB concentration. The large standard deviations at high equilibrium concentration were related to the random fiber morphology of Bio-KLB-C, where random locations of reaction sites induced deviations in the equilibrium adsorption capability.

Table 4

Parameters for Fitting Adsorption Isotherm of Bio-KLB-C

Langmuir model			Freundlich model		
q_{max} (mg/g)	K_L (L/mg)	R^2	n	$K_F\left(\mathrm{mg}^{1-1/n}\mathrm{L}^{1/n}/\mathrm{g}\right)$	R^2
548.65	0.02	0.98	0.88	5.16	0.98

Both Langmuir and Freundlich models fitted the adsorption isotherm data well with the same correlation coefficient ($R^2 = 0.98$). The Langmuir equilibrium constant was small ($K_L < 1$), demonstrating that adsorption of MB on Bio-KLB-C was favorable [35]. The maximum adsorption capacity determined from Langmuir adsorption isotherm model was 548.65 mg/g, higher than the maximum value of 222.95±132.80 mg/g obtained for the range of MB concentration considered in the experiments. It is worth noting that this equilibrium adsorption capacity (222.95 mg/g) was higher than that of electrospun commercial activated carbon and similar CFs produced from commercial lignin [24]. Comparing to other works in Table 5, the maximum equilibrium adsorption capacity of MB on Bio-KLB-C (548.65 mg/g) surpassed most other CF adsorbents made from electrospun bioresource fibers. Even though it may not reach the adsorption capacity of MB on commercial activated carbon (980.3 mg/g), its research potential as a bioresource alternative to activated carbon is immense [60].

After fitting using Freundlich adsorption isotherm model, $K_F = 0.02$ L/mg, the mass of MB adsorbed at unit equilibrium MB concentration ($C_e = 1$), was obtained [61]. The heterogeneity

17

factor n measures the adsorption intensity and was found to be 0.88 in this work. The value of $1/n$ larger than 1 suggested cooperative adsorption, where adsorbed MB molecules facilitated subsequent adsorption from the solution [62,63].

Table 5

Maximum adsorption capacity of MB on electrospun bio-based CFs reported in other investigations

Precursor	Maximum adsorption capacity (mg/g)	Reference
Commercial lignin-based CF	220	24
Coconut shell charcoal derived CF	166.67	64
Bagasse CF	15.6	65
Cellulose derived CF/carbon black	84.6	66
Bio-KLB-C	548.65	This work

3.4.4. Cyclic Adsorption

It is imperative to evaluate the reusability of adsorbent for economical application in water treatment. The reusability of Bio-KLB-C was assessed for 5 cycles of adsorption-desorption process. The cyclic adsorption efficiency of Bio-KLB-C is shown in Figure 6b, which reduced below 80% after four cycles and decreased to 75% after the fifth cycle. The recyclability of Bio-KLB-C was decent for MB adsorption. Overall, Bio-KLB-C is an auspicious novel adsorbent material for dye adsorption in water treatment.
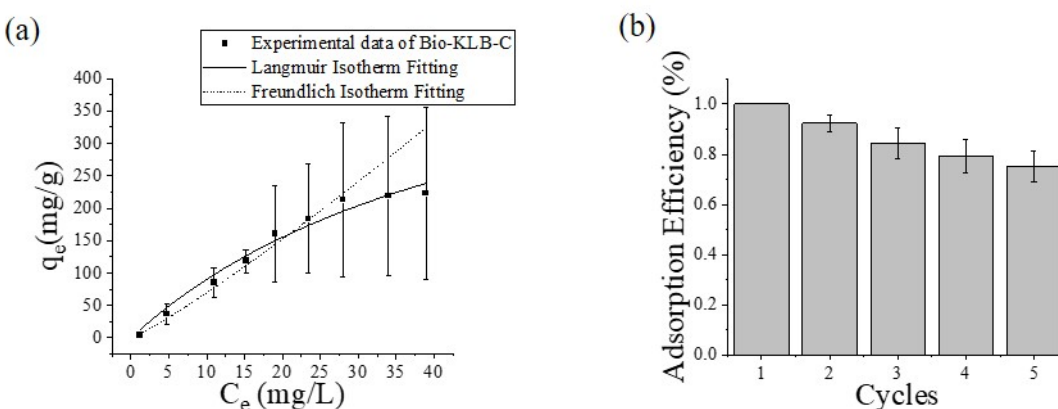
Figure 6. (a) Adsorption isotherm of MB on Bio-KLB-C, fitted with Langmuir adsorption isotherm and Freundlich adsorption isotherm models, (b) adsorption efficiency in cyclic adsorption tests of MB on Bio-KLB-C

Since Bio-KLB-C exhibited exceptional mechanical properties, it can be considered for other applications such as membrane filtration or supercapacitor electrodes. In terms of water treatment, the potential usage of Bio-KLB-C in the removal of metals, oil, or other dyes can be investigated in future works. Conducting nitrogen adsorption analysis to characterize the specific surface area and the pore size distribution of KLA-C and Bio-KLB-C will be beneficial to further confirm the mechanism of their MB adsorption capacities.

4. Conclusion

This work introduces a novel sustainable adsorbent material, electrospun bio-cleaned lignin-based carbon fibers, and provides a comprehensive study on its application in MB adsorption. Submicron carbon fibers were successfully produced from Bio-KLB via electrospinning. Bio-cleaning substantially enhanced spinnability of KLB, converting KLB from un-spinnable to electrospinnable material. The carbonized Bio-KLB fibers showed 34% reduction in fiber diameter, 3-times increase in elastic modulus, and 2-times increase in tensile strength. The average fiber diameter of Bio-KLB carbon fibers was 278.95 ± 49.89 nm. The small-diameter fibers increased specific surface area of the fiber mat and the porous structure facilitated adoption mechanism towards dye molecules. Bio-KLB carbon fibers exhibited excellent adsorption of methylene blue (MB). Kinetic adsorptions of MB on Bio-KLB carbon fibers showed good agreement with pseudo-first-order model. This work has demonstrated a novel strategy to use electrospun bacteria-purified lignin-based carbon fibers in methylene blue adsorption. Electrospun Bio-KLB carbon fiber is a potential low-cost alternative to activated carbon in wastewater treatment and a strong candidate in the development of next-generation sustainable adsorbent material.

Conflict of Interest

The authors declare there is no financial or personal relationship that could influence their works in this paper.

Acknowledgement

References

(1)   Yaseen, D. A.; Scholz, M. *Textile Dye Wastewater Characteristics and Constituents of Synthetic Effluents: A Critical Review*; Springer Berlin Heidelberg, 2019; Vol. 16. https://doi.org/10.1007/s13762-018-2130-z.

(2)   Sun, B.; He, Z.; Hou, Q.; Liu, Z.; Cha, R.; Ni, Y. Interaction of a Spirooxazine Dye with Latex and Its Photochromic Efficiency on Cellulosic Paper. *Carbohydr. Polym.* **2013**, *95* (1), 598–605. https://doi.org/10.1016/j.carbpol.2013.03.032.

(3)   Velho, S. R. K.; Brum, L. F. W.; Petter, C. O.; dos Santos, J. H. Z.; Šimunić, Š.; Kappa, W. H. Development of Structured Natural Dyes for Use into Plastics. *Dye. Pigment.* **2017**, *136*, 248–254. https://doi.org/10.1016/j.dyepig.2016.08.021.

(4)   Michaëlsson, G.; Juhlin, L. Urticaria Induced by Preservatives and Dye Additives in Food and Drugs. *Br. J. Dermatol.* **1973**, *88* (6), 525–532. https://doi.org/10.1111/j.1365-2133.1973.tb08014.x.

(5)   Liu, L.; He, D.; Pan, F.; Huang, R.; Lin, H.; Zhang, X. Comparative Study on Treatment of Methylene Blue Dye Wastewater by Different Internal Electrolysis Systems and COD Removal Kinetics, Thermodynamics and Mechanism. *Chemosphere* **2020**, *238*, 124671. https://doi.org/10.1016/j.chemosphere.2019.124671.

(6)   Mohammed MA; Shitu A; Ibrahim A. Removal of Methylene Blue Using Low Cost Adsorbent: A Review. *Res. J. Chem. Sci.* **2014**, *4* (1), 91–102.

(7)   Pathania, D.; Sharma, S.; Singh, P. Removal of Methylene Blue by Adsorption onto Activated Carbon Developed from Ficus Carica Bast. *Arab. J. Chem.* **2017**, *10*, S1445–S1451. https://doi.org/10.1016/j.arabjc.2013.04.021.

(8)   Pandit, P.; Basu, S. Removal of Ionic Dyes from Water by Solvent Extraction Using Reverse Micelles. *Environ. Sci. Technol.* **2004**, *38* (8), 2435–2442. https://doi.org/10.1021/es030573m.

(9)   Marshall, P. N.; Lewis, S. M. The Purification of Methylene Blue and Azure b by Solvent Extraction and Crystallization. *Biotech. Histochem.* **1975**, *50* (6), 375–381. https://doi.org/10.3109/10520297509117095.

(10)   El Hajj Hassan, M. A.; El Jamal, M. M. Kinetic Study of the Electrochemical Oxidation of Methylene Blue with Pt Electrode. *Port. Electrochim. Acta* **2013**, *30* (5), 351–359. https://doi.org/10.4152/pea.201205351.

(11)   El-Katori, E. E.; Ahmed, M. A.; El-Bindary, A. A.; Oraby, A. M. Impact of CdS/SnO2heterostructured Nanoparticle as Visible Light Active Photocatalyst for the Removal Methylene Blue Dye. *J. Photochem. Photobiol. A Chem.* **2020**, *392* (January), 112403. https://doi.org/10.1016/j.jphotochem.2020.112403.

(12)   Bielska, M.; Szymanowski, J. Removal of Methylene Blue from Waste Water Using Micellar Enhanced Ultrafiltration. *Water Res.* **2006**, *40* (5), 1027–1033. https://doi.org/10.1016/j.watres.2005.12.027.

(13)   Gupta, V. K.; Kumar, R.; Nayak, A.; Saleh, T. A.; Barakat, M. A. Adsorptive Removal of Dyes from Aqueous Solution onto Carbon Nanotubes: A Review. *Adv. Colloid Interface Sci.* **2013**, *193–194*, 24–34. https://doi.org/10.1016/j.cis.2013.03.003.

(14)   Zhang, C.; Dai, Y.; Wu, Y.; Lu, G.; Cao, Z.; Cheng, J.; Wang, K.; Yang, H.; Xia, Y.; Wen, X.; Ma, W.; Liu, C.; Wang, Z. Facile Preparation of Polyacrylamide/Chitosan/Fe3O4 Composite Hydrogels for Effective Removal of Methylene Blue from Aqueous Solution. *Carbohydr. Polym.* **2020**, *234* (January), 115882. https://doi.org/10.1016/j.carbpol.2020.115882.

(15)   Yagub, M. T.; Sen, T. K.; Afroze, S.; Ang, H. M. Dye and Its Removal from Aqueous Solution by Adsorption: A Review. *Adv. Colloid Interface Sci.* **2014**, *209*, 172–184. https://doi.org/10.1016/j.cis.2014.04.002.

(16)   Ghaedi, M.; Nasab, A. G.; Khodadoust, S.; Rajabi, M.; Azizian, S. Application of Activated Carbon as Adsorbents for Efficient Removal of Methylene Blue: Kinetics and Equilibrium Study. *J. Ind. Eng. Chem.* **2014**, *20* (4), 2317–2324. https://doi.org/10.1016/j.jiec.2013.10.007.

(17)   Hameed, B. H.; Din, A. T. M.; Ahmad, A. L. Adsorption of Methylene Blue onto Bamboo-Based Activated Carbon: Kinetics and Equilibrium Studies. *J. Hazard. Mater.* **2007**, *141* (3), 819–825. https://doi.org/10.1016/j.jhazmat.2006.07.049.

(18)   Ma, X.; Zhang, F.; Zhu, J.; Yu, L.; Liu, X. Preparation of Highly Developed Mesoporous Activated Carbon Fiber from Liquefied Wood Using Wood Charcoal as Additive and Its Adsorption of Methylene Blue from Solution. *Bioresour. Technol.* **2014**, *164*, 1–6. https://doi.org/10.1016/j.biortech.2014.04.050.

(19)   Wen, X.; Liu, H.; Zhang, L.; Zhang, J.; Fu, C.; Shi, X.; Chen, X.; Mijowska, E.; Chen, M. J.; Wang, D. Y. Large-Scale Converting Waste Coffee Grounds into Functional Carbon

Materials as High-Efficient Adsorbent for Organic Dyes. *Bioresour. Technol.* **2019**, *272* (October 2018), 92–98. https://doi.org/10.1016/j.biortech.2018.10.011.

(20)   Bengtsson, A.; Bengtsson, J.; Olsson, C.; Sedin, M.; Jedvert, K.; Theliander, H.; Sjöholm, E. Improved Yield of Carbon Fibres from Cellulose and Kraft Lignin. *Holzforschung* **2018**, *72* (12), 1007–1016. https://doi.org/10.1515/hf-2018-0028.

(21)   Vakkilainen, E.; Välimäki, E. Effect of Lignin Separation to Black Liquor and Recovery Boiler Operation. *TAPPI Press - TAPPI Eng. Pulping Environ. Conf. 2009 - Innov. Energy, Fiber Compliance* **2009**, *3* (November 2014), 1515–1556. https://doi.org/10.13140/2.1.2039.6485.

(22)   Zhao, R.; Wang, Y.; Li, X.; Sun, B.; Wang, C. Synthesis of β-Cyclodextrin-Based Electrospun Nanofiber Membranes for Highly Efficient Adsorption and Separation of Methylene Blue. *ACS Appl. Mater. Interfaces* **2015**, *7* (48), 26649–26657.

(23)   Jain, A.; Balasubramanian, R.; Srinivasan, M. P. Hydrothermal Conversion of Biomass Waste to Activated Carbon with High Porosity: A Review. *Chem. Eng. J.* **2016**, *283*, 789–805. https://doi.org/10.1016/j.cej.2015.08.014.

(24)   Beck, R. J.; Zhao, Y.; Fong, H.; Menkhaus, T. J. Electrospun Lignin Carbon Nanofiber Membranes with Large Pores for Highly Efficient Adsorptive Water Treatment Applications. *J. Water Process Eng.* **2017**, *16*, 240–248. https://doi.org/10.1016/j.jwpe.2017.02.002.

(25)   Yao, Y.; Xu, F.; Chen, M.; Xu, Z.; Zhu, Z. Adsorption Behavior of Methylene Blue on Carbon Nanotubes. *Bioresour. Technol.* **2010**, *101* (9), 3040–3046. https://doi.org/10.1016/j.biortech.2009.12.042.

(26)   Ghosh, T.; Ngo, T.-D.; Kumar, A.; Ayranci, C.; Tang, T. Cleaning Carbohydrate Impurities from Lignin Using Pseudomonas Fluorescens. *Green Chem.* **2019**, *21* (7), 1648–1659.

(27)   Ghosh, T.; Chen, J.; Kumar, A.; Tang, T.; Ayranci, C. Bio-Cleaning Improves the Mechanical Properties of Lignin-Based Carbon Fibers. *RSC Adv.* **2020**, *10* (39), 22983–22995.

(28)   Aslanzadeh, S.; Ahvazi, B.; Boluk, Y.; Ayranci, C. Carbon Fiber Production from Electrospun Sulfur Free Softwood Lignin Precursors. *J. Eng. Fiber. Fabr.* **2017**, *12* (4), 33–43. https://doi.org/10.1177/155892501701200405.

(29)   Hotaling, N. A.; Bharti, K.; Kriel, H.; Simon, C. G. DiameterJ: A Validated Open Source Nanofiber Diameter Measurement Tool. *Biomaterials* **2015**, *61*, 327–338. https://doi.org/10.1016/j.biomaterials.2015.05.015.

(30)   Ziabari, M.; Mottaghitalab, V.; Haghi, A. K. Evaluation of Electrospun Nanofiber Pore Structure Parameters. *Korean J. Chem. Eng.* **2008**, *25* (4), 923–932. https://doi.org/10.1007/s11814-008-0151-x.

(31)   Yan, H.; Li, H.; Yang, H.; Li, A.; Cheng, R. Removal of Various Cationic Dyes from Aqueous Solutions Using a Kind of Fully Biodegradable Magnetic Composite Microsphere. *Chem. Eng. J.* **2013**, *223*, 402–411. https://doi.org/10.1016/j.cej.2013.02.113.

(32)   Moradi, E.; Ebrahimzadeh, H.; Mehrani, Z.; Asgharinezhad, A. A. The Efficient Removal of Methylene Blue from Water Samples Using Three-Dimensional Poly (Vinyl Alcohol)/Starch Nanofiber Membrane as a Green Nanosorbent. *Environ. Sci. Pollut. Res.* **2019**, *26* (34), 35071–35081. https://doi.org/10.1007/s11356-019-06400-7.

(33)   Ai, L.; Zhang, C.; Liao, F.; Wang, Y.; Li, M.; Meng, L.; Jiang, J. Removal of Methylene Blue from Aqueous Solution with Magnetite Loaded Multi-Wall Carbon Nanotube: Kinetic, Isotherm and Mechanism Analysis. *J. Hazard. Mater.* **2011**, *198*, 282–290. https://doi.org/10.1016/j.jhazmat.2011.10.041.

(34)   Özer, D.; Dursun, G.; Özer, A. Methylene Blue Adsorption from Aqueous Solution by Dehydrated Peanut Hull. *J. Hazard. Mater.* **2007**, *144* (1–2), 171–179. https://doi.org/10.1016/j.jhazmat.2006.09.092.

(35)   Cazetta, A. L.; Vargas, A. M. M.; Nogami, E. M.; Kunita, M. H.; Guilherme, M. R.; Martins, A. C.; Silva, T. L.; Moraes, J. C. G.; Almeida, V. C. NaOH-Activated Carbon of High Surface Area Produced from Coconut Shell: Kinetics and Equilibrium Studies from the Methylene Blue Adsorption. *Chem. Eng. J.* **2011**, *174* (1), 117–125. https://doi.org/10.1016/j.cej.2011.08.058.

(36)   Senthil Kumar, P.; Ramalingam, S.; Senthamarai, C.; Niranjanaa, M.; Vijayalakshmi, P.; Sivanesan, S. Adsorption of Dye from Aqueous Solution by Cashew Nut Shell: Studies on Equilibrium Isotherm, Kinetics and Thermodynamics of Interactions. *Desalination* **2010**, *261* (1–2), 52–60. https://doi.org/10.1016/j.desal.2010.05.032.

(37)   Johnson, D. J.; Tomizuka, I.; Watanabe, O. The Fine Structure of Lignin-Based Carbon Fibres. **1975**, *13*, 321–325.

(38) Schlee, P.; Hosseinaei, O.; Baker, D.; Landmér, A.; Tomani, P.; Mostazo-López, M. J.; Cazorla-Amorós, D.; Herou, S.; Titirici, M. M. From Waste to Wealth: From Kraft Lignin to Free-Standing Supercapacitors. *Carbon N. Y.* **2019**, *145*, 470–480. https://doi.org/10.1016/j.carbon.2019.01.035.

(39) Aslanzadeh, S.; Zhu, Z.; Luo, Q.; Ahvazi, B.; Boluk, Y.; Ayranci, C. Electrospinning of Colloidal Lignin in Poly(Ethylene Oxide) N, N-dimethylformamide Solutions. *Macromol. Mater. Eng.* **2016**, *301* (4), 401–413. https://doi.org/10.1002/mame.201500317.

(40) Aslanzadeh, S.; Ahvazi, B.; Boluk, Y.; Ayranci, C. Morphologies of Electrospun Fibers of Lignin in Poly(Ethylene Oxide)/N, N-dimethylformamide. *J. Appl. Polym. Sci.* **2016**, *133* (44).

(41) Bazargan, A. M.; Keyanpour-rad, M.; Hesari, F. A.; Ganji, M. E. A Study on the Microfiltration Behavior of Self-Supporting Electrospun Nanofibrous Membrane in Water Using an Optical Particle Counter. *Desalination* **2011**, *265* (1–3), 148–152. https://doi.org/10.1016/j.desal.2010.07.045.

(42) Casper, C. L.; Stephens, J. S.; Tassi, N. G.; Chase, D. B.; Rabolt, J. F. Controlling Surface Morphology of Electrospun Polystyrene Fibers: Effect of Humidity and Molecular Weight in the Electrospinning Process. *Macromolecules* **2004**, *37* (2), 573–578. https://doi.org/10.1021/ma0351975.

(43) Gao, B.; Yu, H.; Wen, J.; Zeng, H.; Liang, T.; Zuo, F.; Cheng, C. Super-Adsorbent Poly(Acrylic Acid)/Laponite Hydrogel with Ultrahigh Mechanical Property for Adsorption of Methylene Blue. *J. Environ. Chem. Eng.* **2021**, *9* (6), 106346. https://doi.org/10.1016/j.jece.2021.106346.

(44) Kaya-Özkiper, K.; Uzun, A.; Soyer-Uzun, S. A Novel Alkali Activated Magnesium Silicate as an Effective and Mechanically Strong Adsorbent for Methylene Blue Removal. *J. Hazard. Mater.* **2022**, *424* (May 2021). https://doi.org/10.1016/j.jhazmat.2021.127256.

(45) Senthilkumaar, S.; Varadarajan, P. R.; Porkodi, K.; Subbhuraam, C. V. Adsorption of Methylene Blue onto Jute Fiber Carbon: Kinetics and Equilibrium Studies. *J. Colloid Interface Sci.* **2005**, *284* (1), 78–82. https://doi.org/10.1016/j.jcis.2004.09.027.

(46) Kavitha, D.; Namasivayam, C. Experimental and Kinetic Studies on Methylene Blue Adsorption by Coir Pith Carbon. *Bioresour. Technol.* **2007**, *98* (1), 14–21. https://doi.org/10.1016/j.biortech.2005.12.008.

(47) Chen, J.; Cesario, T. C.; Rentzepis, P. M. Effect of PH on Methylene Blue Transient States and Kinetics and Bacteria Photoinactivation. *J. Phys. Chem. A* **2011**, *115* (13), 2702–2707. https://doi.org/10.1021/jp110215g.

(48) Putra, E. K.; Pranowo, R.; Sunarso, J.; Indraswati, N.; Ismadji, S. Performance of Activated Carbon and Bentonite for Adsorption of Amoxicillin from Wastewater: Mechanisms, Isotherms and Kinetics. *Water Res.* **2009**, *43* (9), 2419–2430. https://doi.org/10.1016/j.watres.2009.02.039.

(49) Shi, X.; Wang, X.; Tang, B.; Dai, Z.; Chen, K.; Zhou, J. Impact of Lignin Extraction Methods on Microstructure and Mechanical Properties of Lignin-Based Carbon Fibers. *J. Appl. Polym. Sci.* **2018**, *135* (10). https://doi.org/10.1002/app.45580.

(50) Perezdrienko, I. V.; Molodozhenyuk, T. B.; Shermatov, B. E.; Yunusov, M. P. Effect of Carbonization Temperature and Activation on Structural Formation of Active Lignin Carbons. *Russ. J. Appl. Chem.* **2001**, *74* (10), 1650–1652. https://doi.org/10.1023/A:1014844900142.

(51) Vargas, A. M. M.; Cazetta, A. L.; Kunita, M. H.; Silva, T. L.; Almeida, V. C. Adsorption of Methylene Blue on Activated Carbon Produced from Flamboyant Pods (Delonix Regia): Study of Adsorption Isotherms and Kinetic Models. *Chem. Eng. J.* **2011**, *168* (2), 722–730. https://doi.org/10.1016/j.cej.2011.01.067.

(52) Maldhure, A. V.; Ekhe, J. D. Preparation and Characterizations of Microwave Assisted Activated Carbons from Industrial Waste Lignin for Cu(II) Sorption. *Chem. Eng. J.* **2011**, *168* (3), 1103–1111. https://doi.org/10.1016/j.cej.2011.01.091.

(53) Islam, M. S.; Ang, B. C.; Gharehkhani, S.; Afifi, A. B. M. Adsorption Capability of Activated Carbon Synthesized from Coconut Shell. *Carbon Lett.* **2016**, *20* (1), 1–9. https://doi.org/10.5714/CL.2016.20.001.

(54) Karaçetin, G.; Sivrikaya, S.; Imamołlu, M. Adsorption of Methylene Blue from Aqueous Solutions by Activated Carbon Prepared from Hazelnut Husk Using Zinc Chloride. *J. Anal. Appl. Pyrolysis* **2014**, *110* (1), 270–276. https://doi.org/10.1016/j.jaap.2014.09.006.

(55) Liu, X.; He, C.; Yu, X.; Bai, Y.; Ye, L.; Wang, B.; Zhang, L. Net-like Porous Activated Carbon Materials from Shrimp Shell by Solution-Processed Carbonization and H3PO4 Activation for Methylene Blue Adsorption. *Powder Technol.* **2018**, *326*, 181–189. https://doi.org/10.1016/j.powtec.2017.12.034.

(56) Zhang, L.; You, T.; Zhou, T.; Zhou, X.; Xu, F. Interconnected Hierarchical Porous Carbon from Lignin-Derived Byproducts of Bioethanol Production for Ultra-High Performance Supercapacitors. *ACS Appl. Mater. Interfaces* **2016**, *8* (22), 13918–13925. https://doi.org/10.1021/acsami.6b02774.

(57) Ebadollahzadeh, H.; Zabihi, M. Competitive Adsorption of Methylene Blue and Pb (II) Ions on the Nano-Magnetic Activated Carbon and Alumina. *Mater. Chem. Phys.* **2020**, *248* (February), 122893. https://doi.org/10.1016/j.matchemphys.2020.122893.

(58) Travlou, N. A.; Barczak, M.; Hoffman, J.; Bandosz, T. J. Exploring the Effects of Surface Chemistry on Photosensitivity and Stability of Modified Porous Carbon Textiles. *Carbon N. Y.* **2018**, *131*, 1–9. https://doi.org/10.1016/j.carbon.2018.01.065.

(59) Li, K.; Zhou, M.; Liang, L.; Jiang, L.; Wang, W. Ultrahigh-Surface-Area Activated Carbon Aerogels Derived from Glucose for High-Performance Organic Pollutants Adsorption. *J. Colloid Interface Sci.* **2019**, *546*, 333–343.

(60) Kannan, N.; Sundaram, M. M. Kinetics and Mechanism of Removal of Methylene Blue by Adsorption on Various Carbons - A Comparative Study. *Dye. Pigment.* **2001**, *51* (1), 25–40. https://doi.org/10.1016/S0143-7208(01)00056-0.

(61) Fytianos, K.; Voudrias, E.; Kokkalis, E. Sorption-Desorption Behaviour of 2,4-Dichlorophenol by Marine Sediments. *Chemosphere* **2000**, *40* (1), 3–6. https://doi.org/10.1016/S0045-6535(99)00214-3.

(62) Franca, A. S.; Oliveira, L. S.; Ferreira, M. E. Kinetics and Equilibrium Studies of Methylene Blue Adsorption by Spent Coffee Grounds. *Desalination* **2009**, *249* (1), 267–272. https://doi.org/10.1016/j.desal.2008.11.017.

(63) Liu, S. Cooperative Adsorption on Solid Surfaces. *J. Colloid Interface Sci.* **2015**, *450*, 224–238. https://doi.org/10.1016/j.jcis.2015.03.013.

(64) Widiyastuti, W.; Fahrudin Rois, M.; Suari, N. M. I. P.; Setyawan, H. Activated Carbon Nanofibers Derived from Coconut Shell Charcoal for Dye Removal Application. *Adv. Powder Technol.* **2020**, *31* (8), 3267–3273. https://doi.org/10.1016/j.apt.2020.06.012.

(65) ZabihiSahebi, A.; Koushkbaghi, S.; Pishnamazi, M.; Askari, A.; Khosravi, R.; Irani, M. Synthesis of Cellulose Acetate/Chitosan/SWCNT/Fe3O4/TiO2 Composite Nanofibers for the Removal of Cr(VI), As(V), Methylene Blue and Congo Red from Aqueous Solutions. *Int. J. Biol. Macromol.* **2019**, *140*, 1296–1304.

https://doi.org/10.1016/j.ijbiomac.2019.08.214.

(66)   Gaminian, H.; Montazer, M. Carbon Black Enhanced Conductivity, Carbon Yield and Dye Adsorption of Sustainable Cellulose Derived Carbon Nanofibers. *Cellulose* **2018**, *25* (9), 5227–5240. https://doi.org/10.1007/s10570-018-1929-6.

Table of Contents

A novel methylene blue adsorption material, bio-cleaned electrospun lignin-based carbon fiber, is developed in this study. Lignin is a byproduct from pulp mills and one of the most abundant natural polymers. The fabricated carbon fiber from lignin exhibits substantial adsorption capability of methylene blue, thus it is a sustainable low-cost alternative to activated carbons for water treatment.